International Journal of Nanomedicine

Dovepress
open access to scientific and medical research

Open Access Full Text Article

ORIGINAL RESEARCH

Bone Morphogenetic Protein 7-Loaded Gelatin Methacrylate/Oxidized Sodium Alginate/ Nano-Hydroxyapatite Composite Hydrogel for Bone Tissue Engineering

Shiyuan Huang, Zesen Wang, Xudong Sun, Kuanxin Li

The First Affiliated Hospital of Bengbu Medical University, Bengbu Medical University, Bengbu, Anhui Province, 233044, People's Republic of China

Correspondence: Kuanxin Li, The First Affiliated Hospital of Bengbu Medical University, Bengbu Medical University, Bengbu, Anhui Province, 233044, People's Republic of China, Email kuanxinli@126.com

Background: Bone tissue engineering (BTE) is a promising alternative to autologous bone grafting for the clinical treatment of bone defects, and inorganic/organic composite hydrogels as BTE scaffolds are a hot spot in current research. The construction of nano-hydroxyapatite/gelatin methacrylate/oxidized sodium alginate (nHAP/GelMA/OSA), abbreviated as HGO, composite hydrogels loaded with bone morphogenetic protein 7 (BMP7) will provide a suitable 3D microenvironment to promote cell aggregation, proliferation, and differentiation, thus facilitating bone repair and regeneration.

Methods: Dually-crosslinked hydrogels were fabricated by combining GelMA and OSA, while HGO hydrogels were formulated by incorporating varying amounts of nHAP. The hydrogels were physically and chemically characterized followed by the assessment of their biocompatibility. BMP7-HGO (BHGO) hydrogels were fabricated by incorporating suitable concentrations of BMP7 into HGO hydrogels. The osteogenic potential of BHGO hydrogels was then validated through in vitro experiments and using rat femoral defect models.

Results: The addition of nHAP significantly improved the physical properties of the hydrogel, and the composite hydrogel with 10% nHAP demonstrated the best overall performance among all groups. The selected concentration of HGO hydrogel served as a carrier for BMP7 loading and was evaluated for its osteogenic potential both in vivo and in vitro. The BHGO hydrogel demonstrated superior in vitro osteogenic induction and in vivo potential for repairing bone tissue compared to the outcomes observed in the blank control, BMP7, and HGO groups.

Conclusion: Using hydrogel containing 10% HGO appears promising for bone tissue engineering scaffolds, especially when loaded with BMP7 to boost its osteogenic potential. However, further investigation is needed to optimize the GelMA, OSA, and nHAP ratios, along with the BMP7 concentration, to maximize the osteogenic potential.

Keywords: composite hydrogel, nanohydroxyapatite, BMP7, bone regeneration, BTE

Introduction

According to statistics, millions of fractures and bone defects occur globally every year due to various types of trauma, infections, bone tumors, bone diseases, and other factors. The pressing need for bone repair solutions has intensified with the rapidly aging population.[1] Smaller bone defects can heal naturally through bone remodeling, relying on the body's bone renewal processes. However, surgical reconstruction of supercritical bone defects has been a major challenge for orthopedic surgeons.[2] Bone grafts (autografts and allografts) are often required to help reconstruct bone defects and restore normal function. Autogenous bone grafts are considered the gold standard but have limitations like limited donors and potential complications at the donor site. Allogeneic bone grafts, while conveniently available, pose risks such as immune rejection and potential pathogen transmission.[3] Designing and synthesizing an artificial bionic bone scaffold with unique mechanical and chemical properties for the treatment of bone defects is a promising approach.

Received: 30 January 2024
Accepted: 12 June 2024
Published: 25 June 2024

An ideal bone tissue engineering scaffold should meet the following criteria: (1) should be non-toxic, non-immunogenic, and biocompatible; (2) should possess a porous structure; (3) exhibit sufficient mechanical strength and stability; and (4) degrade at a rate similar to that of the developing bone tissue.[4] Hydrogel is a physically or chemically crosslinked three-dimensional polymer structure with excellent water absorption and retention capacity.[5] Hydrogels have received extensive attention for tissue engineering applications due to their dynamic functional attributes, natural extracellular matrix (ECM)-like characteristics, and their ability to create ecological niches that regulate cell attachment, proliferation, cell-matrix interactions, intercellular communication, and other relevant functions.[6] In addition, hydrogels have favorable osteoinductive activity.[7,8]

Natural polymers are mainly derived from natural proteins or polysaccharide-based biopolymers, with the majority of them being highly biocompatible. Natural polymers such as gelatin and sodium alginate have been widely studied and applied as bone grafting materials.[9] Gelatin methacryloyl (GelMA) has become a popular biomaterial for bone tissue engineering due to its excellent biocompatibility, tunable physical characteristics, and structure similar to natural bone.[9,10] Serum alginate (SA) has a good safety profile and is non-immunogenic, in addition to excellent gelling ability, making it a preferred scaffold material for use in tissue engineering applications.[11] Oxidized sodium alginate (OSA) or partially oxidized alginate obtained by alginate modification contains a large number of aldehyde groups, with which the residual amino groups on GelMA can undergo a dynamic Schiff base reaction, resulting in the synthesis of a composite hydrogel with superior physical properties. Xing et al investigated the Schiff base reaction between adipic dihydrazide-modified gelatin (Gel-ADH) and OSA, developing an injectable hydrogel tissue binder. This binder showcased a suitable swelling rate, excellent injectability, and improved adhesion, along with outstanding biocompatibility.[12]

Hydrogels from a single natural polymer source have the disadvantage of low mechanical strength, thus the combination of bioactive natural polymers with mechanically tough synthetic polymers allows for the preparation of hybrid hydrogels that are more favorable for the repair of bone and cartilage defects.[13] Hydrogel scaffolds fabricated by a combination of gelatin-alginate and cerium nano-composite (GA-nCeO_2) have demonstrated potential as bone tissue engineering scaffolds, with outstanding performance, especially for bone defects.[14] Hydroxyapatite (HAp) is a major mineral constituent of human bone tissue. Due to its outstanding osteoconductive, osteoinductive, and cell adhesion features, alongside its potential for drug delivery, this material stands out as a promising option in bone tissue engineering applications.[15] Nanoscale hydroxyapatite maximally mimics the microstructure of human bone tissue with significantly enhanced fracture toughness and mechanical strength. At the same time, the reduction of crystalline particles results in a larger surface area of the material, which is more conducive to the formation of chemical bonds with other organic skeletal materials.[16] Biosynthetic scaffolds fabricated using nanohydroxyapatite particles as fillers have been found to prompt osteogenic differentiation of stem cells.[5] Nanomaterials, when used to load and release drugs, offer increased storage capacity for drugs due to their unique structural attributes that directly impact drug release behavior.[17] The incorporation of rhBMP-2 into nanohydroxyapatite (nHAP) has proven effective in reducing initial burst release and prolonging retention time at the bone injury site.[18] Bone morphogenetic proteins 7 (BMP7), also known as osteogenic protein-1 (OP-1), have been shown to have osteoinductive activity.[19,20] These proteins attract stem cells to the injury site and stimulate the proliferation and differentiation of osteoblasts.[21] Moreover, in vitro investigations have indicated that BMP7 can impede osteoclast formation by disrupting signaling pathways.[22] Currently, the typical dose of BMP7 is 3.5 mg, which is usually combined with 1 g of bovine collagen particles to serve as a scaffold for bone formation. However, the high economic cost along with a series of side effects including ectopic bone formation, abnormal inflammatory response, nerve damage, and cancer that may arise from a high concentration of the drug has limited the clinical application of BMP7.[23] As a result, appropriate carriers are typically needed to prolong its retention at the site of application, ensuring appropriate dosage and sustained activity.

In this work, GelMA was combined with OSA through a Schiff base reaction, followed by UV irradiation for polycrosslinking. Various amounts of nHAP were introduced, and the resulting composite hydrogel was used to synthesize the BHGO hydrogel by incorporating an appropriate concentration of BMP7. Physical characterization and performance assessment were used to select the suitable composite hydrogel. Rat bone marrow-derived mesenchymal stem cells (BMSCs) were employed for in vitro experiments to assess the osteogenic differentiation induced by BHGO. Further, a rat distal femur defect model was utilized to evaluate the osteogenic potential of BHGO. The osteogenic

potential of the composite hydrogel was ultimately evaluated through a rat distal femur defect model. These preliminary findings aim to introduce novel concepts for scaffold design in bone tissue engineering and offer a fresh perspective for the clinical treatment of bone defects.

Materials and Methods

Materials

SA, Gel, nHAP (EFL, Suzhou, China); PBS, trypsin, penicillin and streptomycin mixture (100×) (Taiwan, Shanghai, China); Extra-grade fetal bovine serum (FBS) and F12 medium (JZD, Bengbu, China); COL1, RUNX2, OPN, and OCN (Abcam, Cambridge, UK). Other reagents and solvents were commercially obtained and used as received without any further purification.

Stent Preparation

Preparation of GelMA

Gelatin was converted into GelMA as described in reference.[24] Initially, 20 g of gelatin was introduced into 150 mL of distilled water at 50 °C. After thorough stirring and complete dissolution, 30 mL of methacrylic anhydride was gradually added, and stirring was continued for 4 hours. The resulting liquid was then transferred into a dialysis membrane (MW cutoff, 3500 Da). The solution was dialyzed against deionized water for 4 days to eliminate any unreacted methacrylic anhydride. Subsequently, the post-dialysis solution underwent freeze-drying, yielding the white foamy GelMA precursor.

Preparation of OSA

Using a method previously described in the literature,[25] 10 g of SA was added to 200 mL of distilled water in the dark and stirred for 1 hour until the SA was completely dissolved. Then, 50 mL of anhydrous ethanol was added to the solution while stirring. A specified amount of $NaIO_4$ (1.5 g) was then added with continuous stirring for 12 h to achieve a target degree of oxidation of approximately 20%. Ethylene glycol (2 mL) was added to neutralize the unreacted NaIO4 in the solution. Subsequently, anhydrous ethanol and 5 g of NaCl were added to precipitate OSA, which was dialyzed with deionized water for 4 days (molecular weight cut-off, 3500 Da). A white, flocculent, loosely aggregated sample of the OSA was obtained by freeze-drying at the end of dialysis. To determine the degree of oxidation, the OSA was analyzed using Fourier-transform infrared (FTIR) spectroscopy, focusing on the characteristic peaks associated with aldehyde groups. Additionally, titration methods were employed to quantify the aldehyde content. The target degree of oxidation was confirmed to be approximately 20% by comparing the experimental results to a calibration curve obtained from standard solutions of known aldehyde content.

Preparation of nHAP/GelMA/OSA (HGO) Hydrogels

The procedure for the preparation of hydrogels involved blending varied quantities of nHAP with a mixture of 10% w/v GelMA and 2% OSA in a PBS solution. The mixture was placed in a water bath at 60 °C for approximately 30 min with periodic shaking until complete dissolution. Following this, Irgacure 2959 (0.5% w/v) was introduced as a photoinitiator, and the mixture was exposed to UV light for 30 seconds (360–480 nm) following stirring. The resulting hydrogels were referred to as 5% HGO, 10% HGO, 15% HGO, and 20% HGO.

Preparation of BMP7-nHAP/GelMA/OSA Hydrogel (BHGO)

Using a method described in the literature,[26] 1 g of nHAP was immersed in 1 mL of rhBMP-7 solution (1 μg/mL) in acetic acid at a concentration of 0.05 mg/mL for 4 h to allow complete absorption. Freeze-drying yielded nHAP loaded with BMP7. BMP7-nHAP was mixed with 10% w/v GelMA and 2% OSA in PBS solution in a water bath at 60 °C for half an hour, during which it was shaken several times until complete dissolution. Irgacure 2959 (0.5% w/v) was added as a photoinitiator. The product was stirred sufficiently and then subjected to ultraviolet light (360~480 nm). BMP7-nHAP/GelMA/OSA hydrogel was obtained by irradiation under UV light (360~480 nm) with sufficient mixing.

Microscopy and Characterization of Hydrogel Scaffolds

Microstructure

The various concentrations of nHAP-containing composite hydrogels underwent freeze-drying followed by liquid nitrogen embrittlement. Subsequently, the Microstructures of each hydrogel group were examined using an S-4800 scanning electron microscope (SEM: Hitachi, Japan) after surface sputtering with gold. The pore size and nanoparticle distribution within each hydrogel group were thus examined.

Mechanical Properties

Hydrogel scaffolds (diameter 8 mm, height 10 mm, n = 3) were fabricated in a mold. The maximum compressive strength and compressive modulus of the hydrogel scaffolds were tested using a universal testing machine wherein the compression speed was set at 5 mm/min. This process involved discontinuing compression once full deformation occurred to obtain stress-strain curves and determine the maximum compressive strength. The compression modulus is derived from the gradient of the stress-strain curve's linear section.

Dissolution Properties

Hydrogel scaffolds (n=3), with a 15 mm diameter and 2 mm height, were prepared. Initially, their weights were measured and noted as W_0. Subsequently, these hydrogels were placed in a 12-well plate, where 3mL of PBS solution was introduced into each well. After different durations, the hydrogels were extracted, excess surface water was carefully removed using filter paper, and their weights were re-measured and documented as W_1. The swelling performance of the hydrogel was examined by calculating its water absorption rate in PBS. The formula for the measurement of swelling property is: swelling rate (%) = W_1 -W_0/W_0 ×100%.

In vitro Degradation Properties

Hydrogel scaffolds (n=3) with a diameter of 8 mm and a height of 10 mm were made, freeze-dried, and weighed as W_0. The hydrogel was placed in a 12-well plate, and 3 mL PBS solution was added to each well. The PBS solution was removed after immersing the hydrogels for different periods of time at 37 °C, following which the hydrogels were freeze-dried, and the weight was recorded as W_1. The PBS was replaced once every 2 days. The formula for measuring the degradation rate is: Degradation rate (%) = (W_0-W_1)/W_0 ×100%.

Cytocompatibility of Hydrogels

Fabrication of Hydrogel Leachate

The procedures adhered to the International Standards Organization (ISO/EN 10993–12). The hydrogels from each group (0%, 5%, 10%, 15%, 20% HGO) were combined with complete medium or osteogenic medium (comprising 50 μg/mL vitamin C, 5 mM sodium β-glycerophosphate, 10 nM dexamethasone, and conditioned medium) at a ratio of 1 g/10 mL. These mixtures were left at 37 °C, with the leachate collected every two days, filtered for residues, and replenished with fresh medium for further hydrogel soaking.

Hydrogel Cell Proliferation Assay

The BMSCs were planted in 96-well plates at a density of 5000 cells/well, and replaced with hydrogel leachate culture after the BMSCs had adhered to the wall. The leachate in the wells was aspirated following 1, 2, and 3 days of incubation, and 100 μL of CCK8 working solution configured in a 1:9 ratio was added. The plates were then incubated in a water bath at 37 °C for 2 hours, after which the optical density (OD) values of each group were measured at 450 nm.

Hydrogel Cell Live/Dead Assay

BMSCs were seeded into 24-well plates at a density of 50,000 cells/well. After cell attachment, the culture medium was replaced with hydrogel leachate for incubation. After 3 days, the hydrogel leachate was aspirated, the cells were rinsed twice with PBS and then incubated with calcein-AM working solution for 40 min. Subsequently, the calcein-AM solution was removed, and the cells were washed twice with PBS. Propidium iodide (PI) working solution was added and incubated for 2 min, followed by removal of the solution and washing of the cells twice with PBS. Finally, the stained

cells in each hydrogel system were observed under a fluorescence microscope. The staining and washing steps were carried out in light protected environment.

Hydrogel Cytoskeleton Experiments

BMSCs were planted in 24-well plates at a density of 50,000 cells/well, and the cells were cultured in hydrogel leachate after wall attachment, after 3 days of culture, 100 nM ghost pen cyclic peptide working solution and DAPI working solution were prepared according to the kit instructions, respectively. The hydrogel leaching solution was removed, washed twice with PBS, and fixed by adding an appropriate amount of 4% paraformaldehyde solution for 20 min. Following the removal of the paraformaldehyde fixative, the cells underwent two washes with PBS and were treated with a 0.5% TritonX-100 solution for an additional 10 min. Subsequently, the TritonX-100 solution was removed, and the cells were washed twice with PBS. They were then stained with ghost pen cyclic Peptide working solution for 60 min. After staining, the solution was removed, and the cells were washed twice with PBS before being stained with DAPI solution for 1 min. Finally, the cellular morphology was observed using a fluorescence microscope after two additional washes with PBS. All staining and washing procedures were conducted in a light-protected environment.

In vitro osteogenic performance experiments

Alizarin Red Staining

The BMSCs were cultured in six-well plates and divided into four groups: the blank group, the BMP7 group, the HGO group, and the BHGO group. Once the cells adhered to the surface, they were treated with specific mediums: osteoinductive medium, osteoinductive medium supplemented with BMP7 (100 ng/mL), 10% HGO leachate, and BHGO leachate, respectively. The medium was replenished every 3 days, and the cells were cultured for 21 days before undergoing alizarin red staining. Following 21-day incubation, the medium was aspirated, and the cells underwent alizarin red staining. Initially, the medium was aspirated, and the cells were thrice washed with PBS. Subsequently, they were fixed with 4% paraformaldehyde at room temperature for 10 min and again washed three times with PBS. Then, 1 mL of 0.1% alizarin red staining solution was added to each well, and they were incubated at room temperature, and protected from light, for 10 min. The excess staining solution was removed by repetitive PBS washes. Finally, the stained cells were observed using an inverted microscope, and images were captured for analysis.

Alkaline Phosphatase (ALP) Staining and Activity Assay

BMSCs from four groups (blank, BMP7, HGO, BHGO) were cultured in six-well plates until they adhered to the surface. Subsequently, they were treated with specific culture mediums: osteoinductive medium, osteoinductive medium supplemented with BMP7 (100 ng/mL), 10% HGO leachate, and BHGO leachate, respectively. The culture media were refreshed every 3 days. After 7 days of culture, ALP staining was conducted. First, the medium was aspirated, and the cells were washed three times with PBS. Then, 4% paraformaldehyde was added to fix the cells at room temperature for 20 min, followed by three washes with PBS. The ALP staining reagent was prepared according to the instructions, and 1 mL of the staining working solution was added to each well. After incubation for 30 min at room temperature, protected from light, the color development was halted by rinsing with deionized water. Finally, the stained cells were observed using an inverted microscope.

After 14 days of incubation, the activity assay was conducted as follows: RIPA lysate (1 mL) was added after removing the culture medium and thoroughly mixing the cells. After transferring the suspension to a centrifuge tube, it was centrifuged at 12,000 rpm for 5 min to collect the supernatant. The working solution, prepared according to the instructions, was then added to the supernatant and incubated in a cell culture incubator for 30 min.

To stop the reaction, a termination solution was added, and the absorbance of the reaction mixture was measured at 405 nm using an enzyme marker.

Western Blot Assay

BMSCs from four groups (blank group, BMP7 group, HGO group, BHGO group) were cultured in Petri dishes until they adhered to the surface. Osteoinductive medium, osteoinductive medium with BMP7 (100 ng/mL), 10% HGO leachate, and BHGO leachate were then added to the corresponding groups for culturing. The culture medium was refreshed every

3 days. After 14 days of culture, total cellular proteins were extracted and subjected to Western blotting to detect the osteogenic markers COL1, RUNX2, OPN, and OCN.

In vivo Osteogenic Properties

Modeling of Critical Defects in the Distal Femur in Rats

Forty healthy male 200–220 g SD rats were randomly assigned to four groups of equal numbers. The rats were weighed and anesthetized by intraperitoneal injection of sodium pentobarbital (30 mg/kg). After administering anesthesia to the rats, they were fixed, and the skin at the lateral thigh site was prepared by sterilization using 1% iodophor. A sterile towel was placed over the area. A longitudinal incision approximately 1.5 cm long was made on the lateral aspect of the distal femur. Ophthalmic scissors were used to gently separate the muscles on both sides, exposing the distal end of the femur. The periosteum at the operation site was removed. Using a handheld drill, the cortex of the rat's distal femur was penetrated, creating a defect approximately 3 mm in diameter and 3 mm in depth. The defects were left untreated in one group, injected with BMP7 in another, and with HGO hydrogel and BHGO hydrogel in the remaining two groups. The muscle membrane, deep fascia, and skin were sutured layer by layer. Epidermal sutures were made to mark the implantation site. Each animal was labeled according to group and fed routinely in separate cages. All rats were injected subcutaneously with penicillin 80,000 U/d for 4 consecutive days to prevent infection. The model rats were anesthetized to death and harvested 4 weeks later.

Radiological Examination

A 5-mm contiguous bone site around the defect was taken and fixed with 4% paraformaldehyde for 36 hours. The osteogenesis of hydrogels in each group was assessed, and a quantitative analysis of new bone formation within the defects was conducted. New bone growth was assessed using Skyscan1172 Micro-CT with parameters set at 80 kV source voltage and 100 μA source current. CTAn software facilitated 3D reconstruction, enabling calculations of various parameters such as defect volume, volume fraction BV/TV (%), trabecular thickness Tb.Th (mm), number of trabeculae Tb.N (1/mm), and trabecular gap Tb.Sp (mm).

Histological Evaluation

A continuous bone site of 5 mm around the femoral defect was taken and immersed in 4% paraformaldehyde solution for 24 h for fixation. Decalcification was carried out using 10% ethylenediaminetetraacetic acid (EDTA). After 4 weeks, the bone underwent dehydration using a series of alcohol gradients. Following this, it was sectioned into slices of 5 μm thickness upon completion of paraffin embedding. These sections were then subjected to histological staining methods such as H&E staining and Masson staining, alongside immunofluorescence chemical staining for the detection of markers like OCN and CD31. This process enabled the observation of new bone formation.

Statistical Methods

All experimental data was statistically analyzed using GraphPad Prism 9.0 and has been presented as mean ± standard deviation. Comparisons between the two groups were made using a *t*-test or unpaired *t*-test, with $p<0.05$ indicating statistical significance.

Results

Hydrogel Preparation

GelMA Results from gelatin's primary amine functionalization by methacrylic acid groups. To regulate the amount of grafted MA and ensure that the amino groups can satisfy both photopolymerization and Schiff base reactions, the degree of methacrylation (DoM) of GelMA was precisely controlled. This was achieved by reacting gelatin with methacrylic anhydride in varying ratios and characterizing the DoM using ^1H NMR spectroscopy. The free amino groups in GelMA were quantified using the TNBS assay to ensure a sufficient number remained for Schiff base formation with OSA. Oxidized alginate, derived from modified alginate, contains numerous aldehyde groups that can undergo aldol-amine condensation with GelMA's unaltered amine groups. Following the addition of the appropriate mass fraction of BMP7-loaded nHAP, UV irradiation of

the composite hydrogel was carried out for 30 seconds. This process involved the photopolymerization of unsaturated bonds within GelMA due to the action of photoinitiators, alongside the dynamic Schiff base reaction between GelMA and OSA, resulting in a dual-crosslinked polymerization network. This optimized hydrogel formulation was tested and shown to be effective in bone repair in a rat femoral defect model, as illustrated in Figure 1.

Hydrogel Morphology and Characterization

External Morphology

The porous structure stands as a crucial feature of hydrogels, with pore size playing a pivotal role in cell recruitment, promoting blood vessel formation, and facilitating nutrient transport. The interior of the hydrogel cross-section was observed via SEM imaging (Figure 2A), showing that GelMA hydrogel, GelMA+OSA hydrogel, and various concentrations of HGO hydrogel exhibited a loose and porous structure. Measurement of the internal pore size of each group of hydrogels (Figure 2B) showed that the pores of GelMA+OSA hydrogels were larger than those of GelMA hydrogels, probably due to the formation of dynamic Schiff base bonds affecting the gel formation process. As the concentration of nHAP increased, the surface of the three-dimensional mesh structure within the hydrogel became progressively rougher. Consequently, the hydrogel's porosity decreased, and its structure grew more compact.

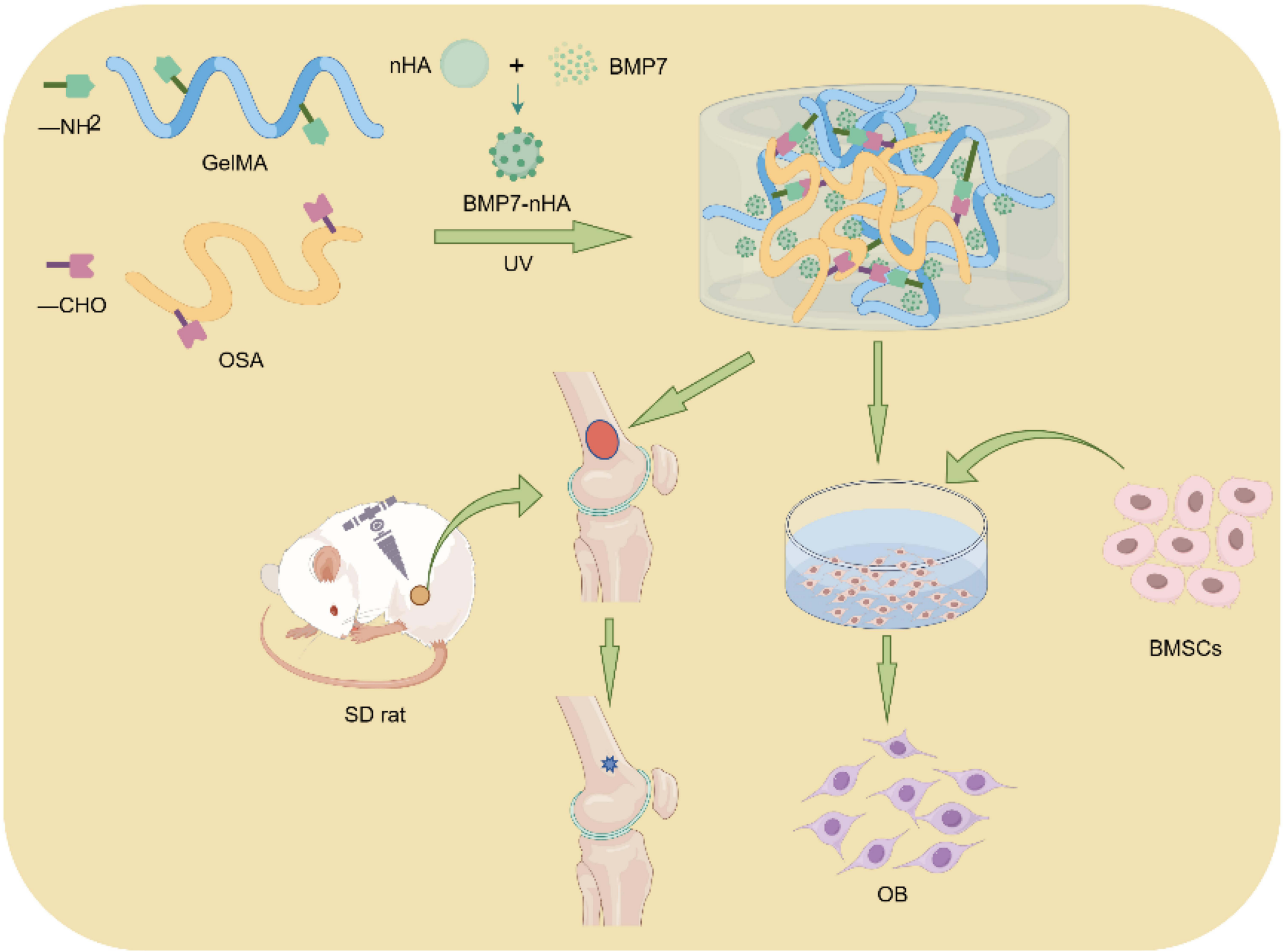

Figure 1 Schematic illustration of the hydrogel preparation process and its application in bone repair. GelMA hydrogels were synthesized by functionalizing gelatin with methacrylic anhydride, followed by characterization of the degree of methacrylation (DoM) using ^1H NMR spectroscopy and quantification of free amino groups via the TNBS assay. The optimized composite hydrogel containing BMP7-loaded nHAP was subjected to UV irradiation to achieve dual-crosslinked polymerization through photopolymerization and Schiff base reactions. The hydrogel formulation was tested in a rat femoral defect model, demonstrating effective bone repair.

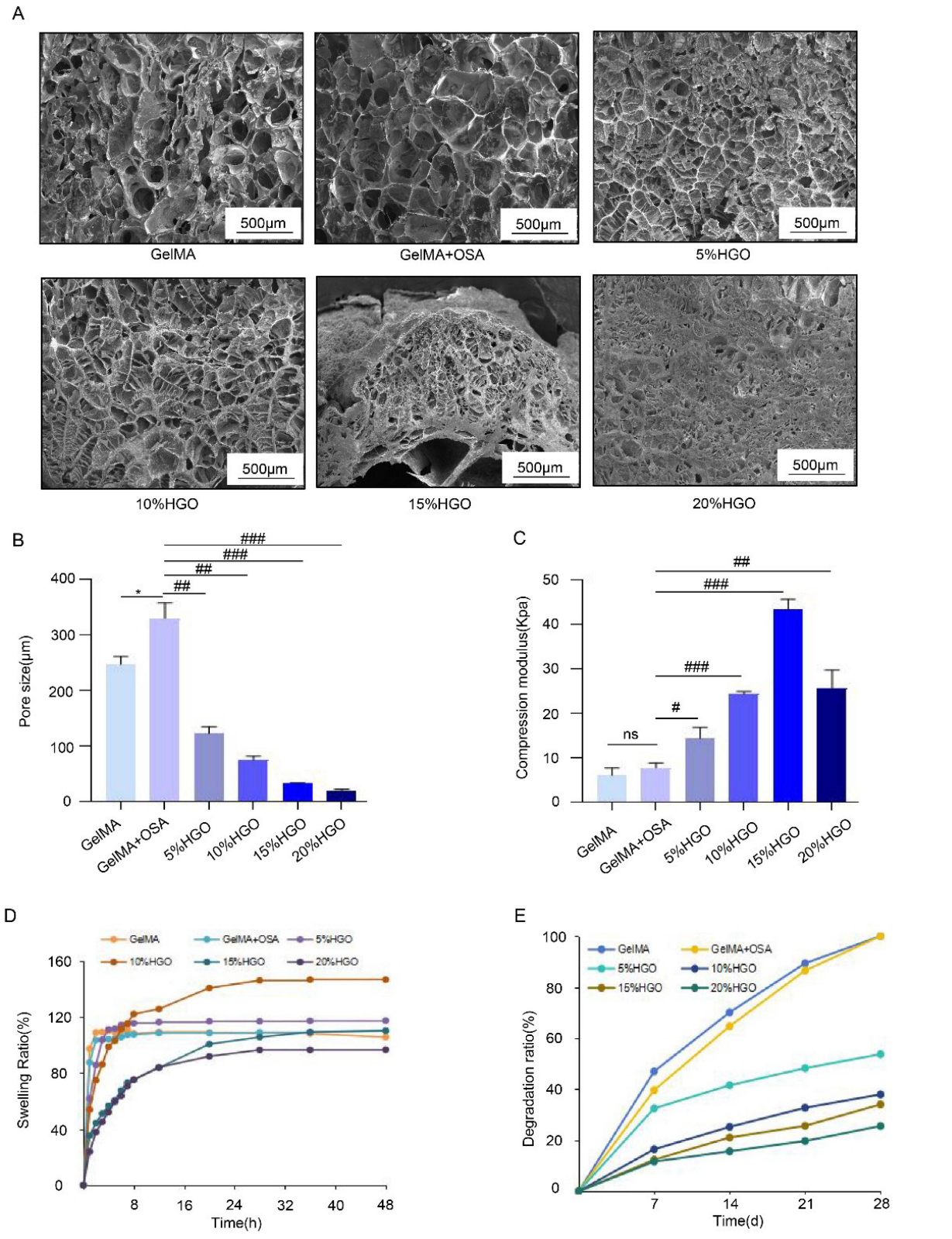

Figure 2 Characterization of hydrogel morphology and mechanical properties.(**A**) SEM images of the cross-sections of GelMA, GelMA+OSA, and HGO hydrogels, displaying a loose and porous structure. (**B**) Quantification of internal pore sizes of each hydrogel group, indicating larger pores in GelMA+OSA hydrogels compared with GelMA hydrogels. (**C**) Compression modulus measurements, illustrating that the inclusion of nHAP strengthened the compression modulus of the hydrogels. (**D**) Swelling behavior of different hydrogel groups, with GelMA and GelMA+OSA hydrogels reaching equilibrium after 2 hours, while nHAP extended swelling time and affected swelling rate. (**E**) Degradation rates of various hydrogel groups over time, showing that nHAP inclusion decelerated the degradation rate. (n =3; nsp>0.05, *p<0.05 compared with GelMA group, #p<0.05, ##p<0.01, ###p<0.005 compared with GelMA+OSA group).

Mechanical Properties

Figure 2C shows the compression modulus of each group of hydrogels. The findings indicated that the incorporation of OSA did not change the compression modulus compared to the GelMA alone group ($n>0.05$). However, the inclusion of nHAP strengthened the compression modulus of the hydrogels ($n<0.05$). Nevertheless, the compression modulus did not consistently escalate with higher nHAP concentrations, as excessively high levels could cause agglomeration, resulting in a reduction of the compression modulus.

The major reason for the agglomeration of nHAP in hydrogel matrices, including GelMA-based systems, primarily stems from its inherent surface properties and high surface energy.[27] Nano-hydroxyapatite particles have a strong tendency to aggregate due to their high surface area-to-volume ratio, which leads to significant van der Waals forces and hydrogen bonding interactions among the particles.[28] Additionally, nHAP particles are prone to agglomeration because of their hydrophilic nature, which causes them to interact strongly with each other rather than dispersing evenly within the hydrophobic or semi-hydrophobic environment of the hydrogel matrix. This issue is exacerbated when the concentration of nHAP is increased, as there are more particles in close proximity, further enhancing the likelihood of particle-particle interactions and agglomeration.[29,30] Agglomeration of nHAP can also be influenced by the lack of adequate surface functionalization. Without appropriate surface modification, such as coating with biocompatible polymers or surfactants, the particles remain highly reactive and tend to form clusters. Surface modification techniques aim to reduce the surface energy and provide steric or electrostatic stabilization to keep the nanoparticles well-dispersed within the hydrogel network.[31] Collectively, the primary reasons for nHAP agglomeration are its high surface energy, hydrophilicity, and the absence of sufficient surface functionalization, which collectively contribute to the challenges in maintaining a uniform dispersion of nHAP in hydrogel systems.

Dissolution Properties

Figure 2D shows the swelling behavior of different groups of hydrogel. GelMA hydrogel and GelMA+OSA hydrogel reached swelling equilibrium after 2 hours of immersion. However, the inclusion of nHAP extended the hydrogel's swelling time to 8 hours and beyond. Notably, nHAP demonstrates outstanding adsorption capacity. The addition of an appropriate quantity of nHAP improved the hydrogel's swelling rate. Yet, excessively high concentrations of nHAP reduced the water absorption capacity, presumably due to the decreased hydrogel porosity associated with high nHAP concentration.

In vitro Degradation Properties

The degradation rate of a scaffold is a critical factor in bone tissue engineering. Premature or delayed degradation can significantly hinder the regeneration of bone tissue. As depicted in Figure 2E, the weight loss percentage was calculated for various hydrogel groups at different time intervals post freeze-drying. GelMA and GelMA+OSA hydrogels underwent complete degradation within four weeks. However, the inclusion of nHAP decelerated the degradation rate, with the composite hydrogel's degradation becoming increasingly delayed with higher nHAP content.

Cell Compatibility of Hydrogels

Cell Proliferation

BMSCs were cultured in each group of hydrogel leachate for 1, 2, and 3 days and then OD results were determined (Figure 3A–C). The findings indicated a progressive increase in cell numbers across all groups over time. Remarkably, the concentrations of HGO demonstrated significantly higher cell counts compared to the GelMA and GelMA/OSA groups ($p<0.05$). This substantiates the excellent biocompatibility of all hydrogel groups.

Cell Viability and Death

Figure 3D shows the staining results of BMSCs after 3 days of incubation in each group of hydrogel leachate. All groups of cells could grow and proliferate normally, with cells having superior viability in 10% and 15% HGO hydrogels.

Cytoskeleton

Figure 3E shows the staining results of each group of BMSCs after 3 days of incubation in the hydrogel leachate, with blue nuclei wrapped by red microfilaments. Compared with the GelMA and GelMA+OSA groups, the number of cells and microfilament structures were significantly higher in the HGO hydrogel.

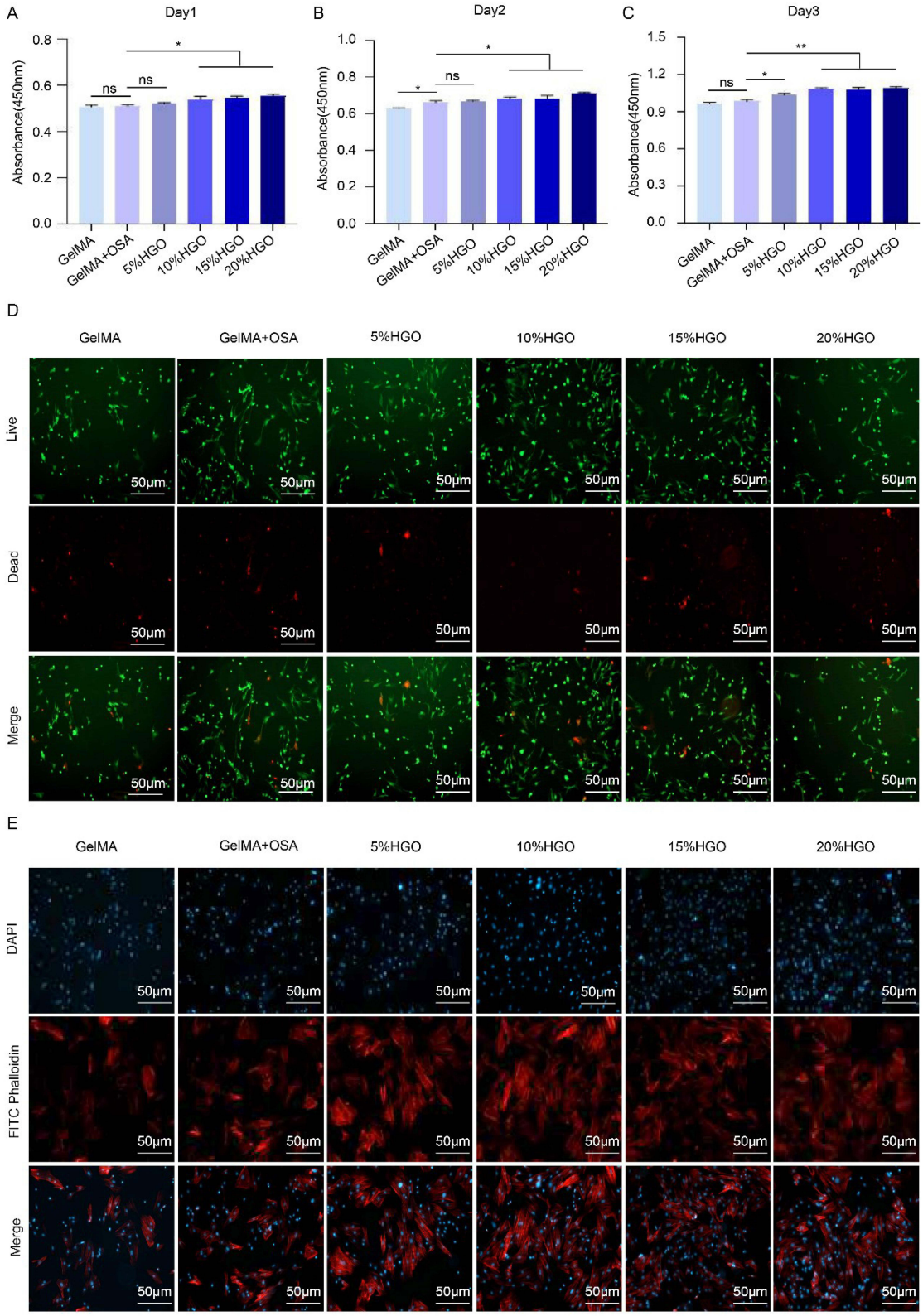

Figure 3 Cell compatibility of hydrogels.(**A–C**) OD measurements of BMSC proliferation in hydrogel leachate over 1, 2, and 3 days, demonstrating a progressive increase in cell numbers, with HGO hydrogels showing significantly higher cell counts. (n =3; nsp>0.05, *p<0.05,**p<0.01 compared with GelMA+OSA group) (**D**) Live/dead staining results of BMSCs after 3 days of incubation, indicating superior cell viability in 10% and 15% HGO hydrogels. (**E**) Cytoskeletal staining of BMSCs after 3 days of incubation, showing a higher number of cells and microfilament structures in HGO hydrogels compared with the GelMA and GelMA+OSA groups.

Osteogenic Differentiation of BMSCs in vitro

Alizarin Red Staining

BMSCs from blank, BMP7, HGO, and BHGO groups were each cultured in osteogenic leachate for 21 days for alizarin red staining, and both gross and inverted microscopy (Figure 4A) showed significantly more osteoid nodules and calcium deposition in BMP7, HGO, and BHGO groups as compared with the blank group. The BHGO group had the highest amount of osteoid nodules and calcium deposition, indicating that the HGO hydrogel can better affect bone differentiation due to the incorporation of BMP7.

Alkaline Phosphatase Staining and Activity

BMSCs from the blank, BMP7, HGO, and BHGO groups were each cultured in osteogenic leachate for 14 days, and the ALP staining results are shown in Figure 4B. Among these groups, the BHGO group exhibited the most intense staining. Correspondingly, in the ALP activity assay results (Figure 4C), the BHGO group displayed the highest ALP activity.

Protein Analysis Techniques

Total cellular protein was extracted from BMSCs belonging to the blank, BMP7, HGO, and BHGO groups following a 14-day culture in osteogenic leachate. Protein analysis was performed to detect the expression levels of COL1, RUNX2, OPN, and OCN in these cells. The protein bands illustrating these expressions are presented in Figure 4D. Quantitative analysis (Figure 4E–H) revealed that the protein expression of these four species in the BMP7, HGO, and BHGO groups surpassed that of the blank control group. Notably, within these groups, the BHGO group exhibited the highest expression levels for all four species compared to the other experimental groups.

Microcomputed Tomography and Analysis

After 4 weeks of modeling, the rat modeled limbs were scanned using Micro CT to observe the healing of the modeled defect sites (Figure 5A). Comparatively, the blank group exhibited the least effective healing, whereas the BHGO group demonstrated the best repair of the bone defect. The ratios of BV/TV (Figure 5B), Tb.Th (Figure 5C), Tb.N (Figure 5D), and Tb.Sp (Figure 5E) to the area of neoplastic bone tissue was calculated to further quantify bone repair and neoplastic bone growth. Among the groups, the BHGO group showed significantly reduced Tb.Sp compared to the other groups ($p< 0.05$). This suggests that both BMP7 and the HGO hydrogel independently aid in bone defect repair, and their combined application proves more effective.

Histologic Examination of Rat Femurs

At the 4th week postoperation, histological examination of the regenerated bone tissue in the defect area was conducted. H&E staining results were consistent with micro-CT reconstructions. Higher magnification showed increased connective and newly formed bone tissues in the BMP7, HGO, and BHGO groups compared to the control group (Figure 6A). Predominantly, the repaired bone defects in the BHGO group exhibited substantial neoplastic bone formation. Masson's trichrome staining (Figure 6B) displayed collagen in bone tissue as blue and other tissues as red. The neoplastic bone tissue area was notably larger in the BMP7, HGO, and BHGO groups in comparison to the control. Importantly, the BHGO group exhibited a larger neoplastic bone tissue area compared to both BMP7 and HGO groups.

Immunofluorescence staining for osteocalcin (OCN), a marker of late osteogenic differentiation, and CD31, a marker of vascular endothelial cells, was performed to assess the ability of different groups to promote osteogenesis and angiogenesis. Figure 6C demonstrated that the staining areas for OCN and CD31 were the largest and most intense in the BHGO group. This finding indicates that BHGO hydrogel scaffolds notably facilitated both new bone formation and neoangiogenesis at the bone defect site.

Discussion

This experimental study verified the safety and ex vivo and in vivo bone repair effects of BHGO hydrogel. HGO hydrogel and BMP7 showed synergistic effects in promoting osteogenic differentiation and bone tissue regeneration in BMSCs.

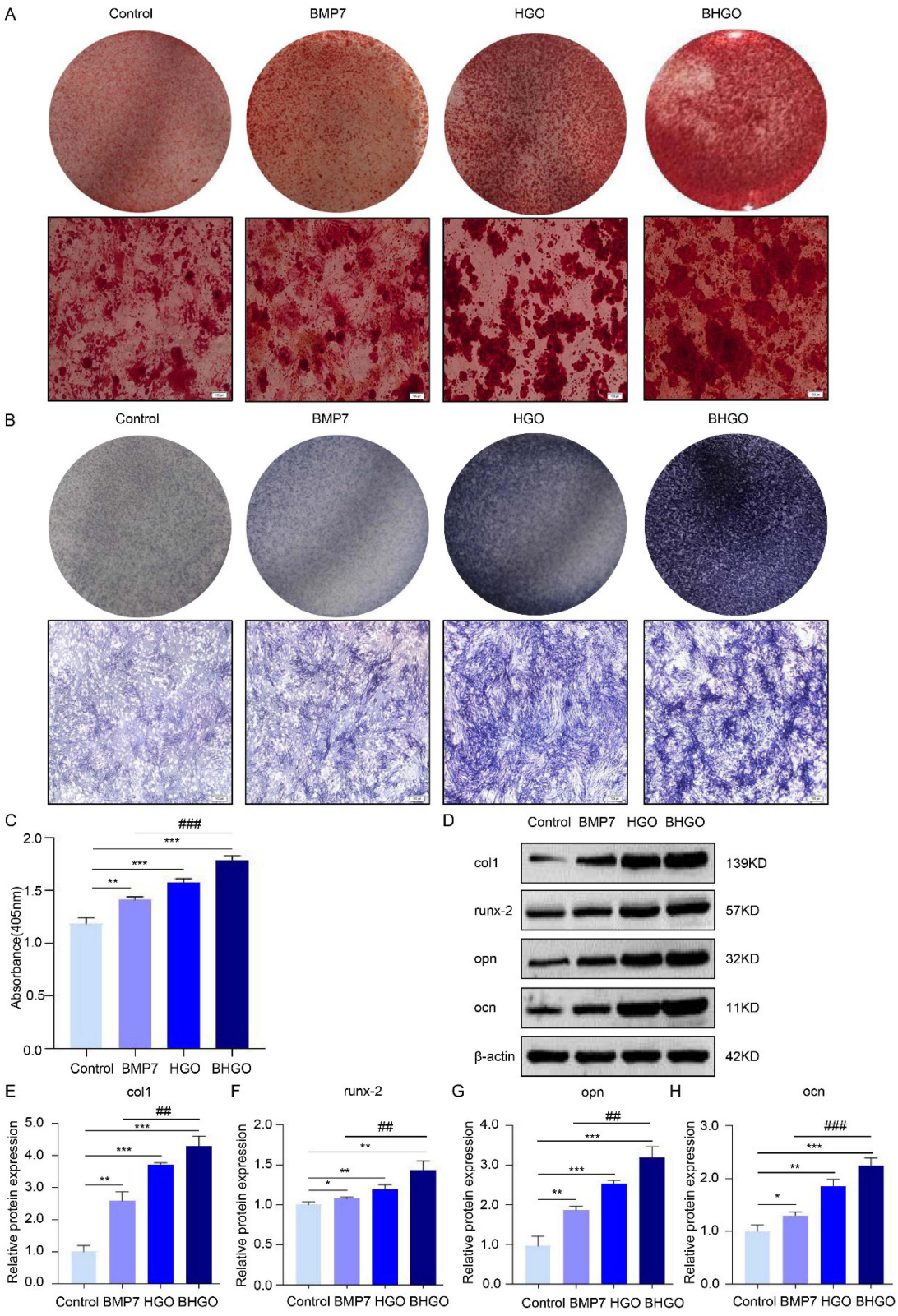

Figure 4 Osteogenic differentiation of BMSCs in vitro.(**A**) Alizarin Red staining of BMSCs after 21 days of culture in osteogenic leachate, displaying more osteoid nodules and calcium deposition in BMP7, HGO, and BHGO groups compared with the blank group. (**B**) ALP staining results of BMSCs after 14 days of culture, with the BHGO group, indicating the most intense staining. (**C**) ALP activity assay results, indicating the highest ALP activity in the BHGO group. (**D**) Protein expression levels of COL1, RUNX2, OPN, and OCN in BMSCs after 14 days of culture, with the highest expression levels observed in the BHGO group. (**E**–**H**) Quantitative analysis of protein expression levels, demonstrating superior osteogenic differentiation in BMP7, HGO, and BHGO groups compared to the blank control group, with the BHGO group showing the highest levels. (n =3; *p<0.05, **p<0.01, ***p<0.005 compared with Control group, #p<0.05, ##p<0.01, ###p<0.005 compared with BMP7 group).

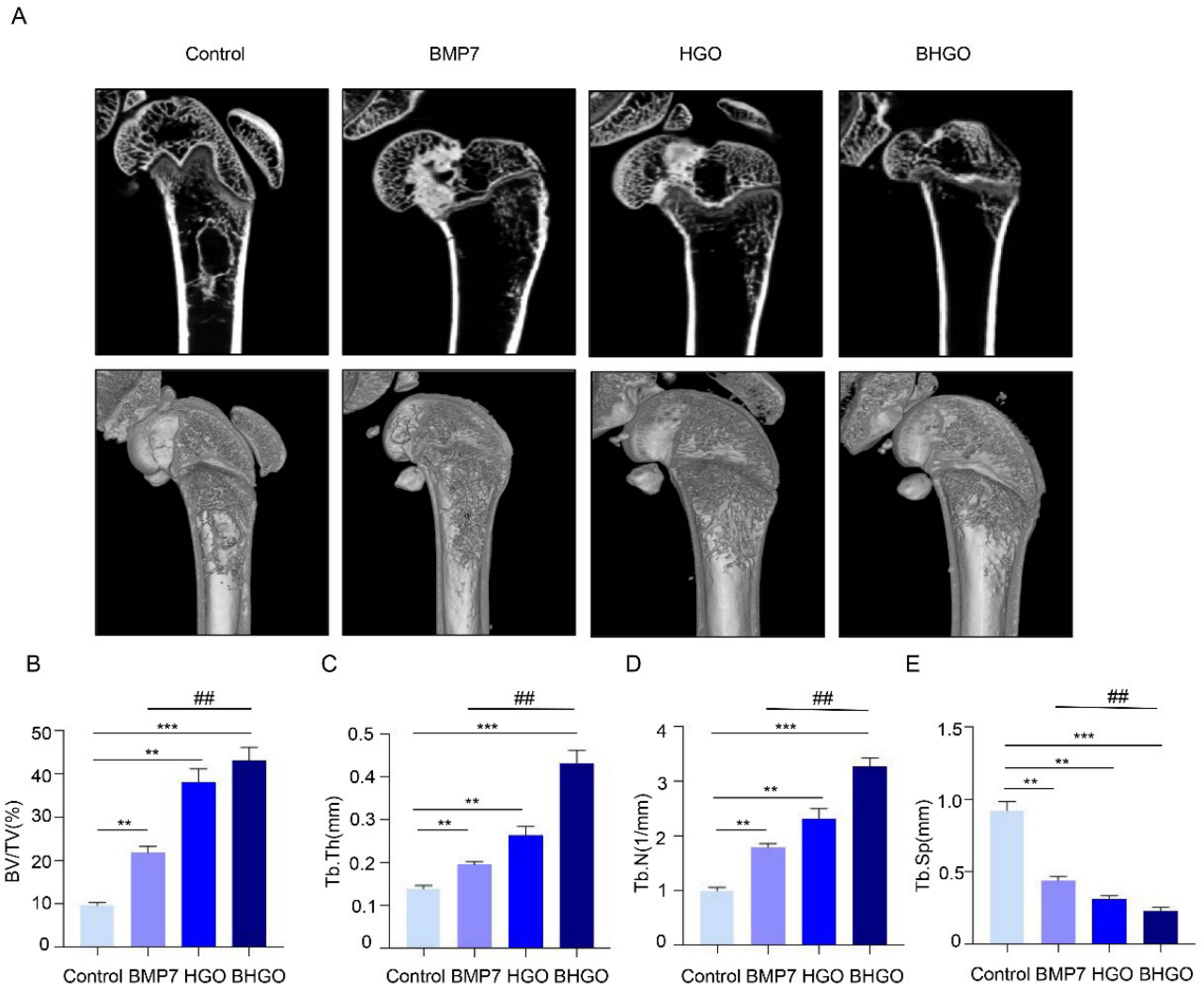

Figure 5 Microcomputed tomography (micro-CT) analysis of bone healing.(**A**) Micro-CT scan of rat modeled limbs after 4 weeks, showing defect site healing in different groups. (**B**) Quantification of bone volume fraction (BV/TV) in neoplastic bone tissue, with the BHGO group showing significant improvement. (**C**) Trabecular thickness (Tb.Th) measurements. (**D**) Trabecular number (Tb.N) measurements. (**E**) Trabecular separation (Tb.Sp) measurements, indicating significantly reduced Tb.Sp in the BHGO group, suggesting enhanced bone defect repair.(n =3; **p<0.01 compared with Control group, ##p<0.01 compared with BMP7 group).

In this experimental study, composite scaffolds were synthesized by the combination of GelMA and OSA through a dynamic Schiff base reaction and photo-crosslinking to form hydrogels carrying different mass fractions of nHAP. The combination of GelMA and OSA facilitates cell recruitment and adhesion on the surface of scaffolds, which provides a space for the growth of new tissues and vascularization.[32,33] nHAP, under its unique nanoarchitecture, can directly serve as a cell adhesion site and significantly enHAPnce the mechanical properties of hydrogels to promote osteogenic differentiation of BMSCs.[34,35] Hydroxyapatite (HA) particles have been reported to stimulate macrophages to secrete angiogenic and osteogenic growth factors.[36] Studies have demonstrated that MSCs exhibit varying differentiation on matrices with different stiffness levels. Notably, BMSCs exhibit osteoblast-like morphology when cultivated on matrices ranging between 25–40 kPa.[37] Accompanied by the increase in nHAP concentration, the hydrogel pore size undergoes gradual shrinking. When the pore size inside the scaffold is extremely small, cell proliferation and migration are adversely affected.[38] Appropriate swelling and degradation rates are also crucial for the scaffold performance. The addition of a suitable concentration of nHAP can increase the composite hydrogel swelling properties.[39] The scaffold's swift water absorption-induced swelling efficiently fills diverse-shaped defects, offering a conducive ground for cell adhesion and proliferation.[20] High-quality scaffolds possess controlled degradation rates aligned with new bone

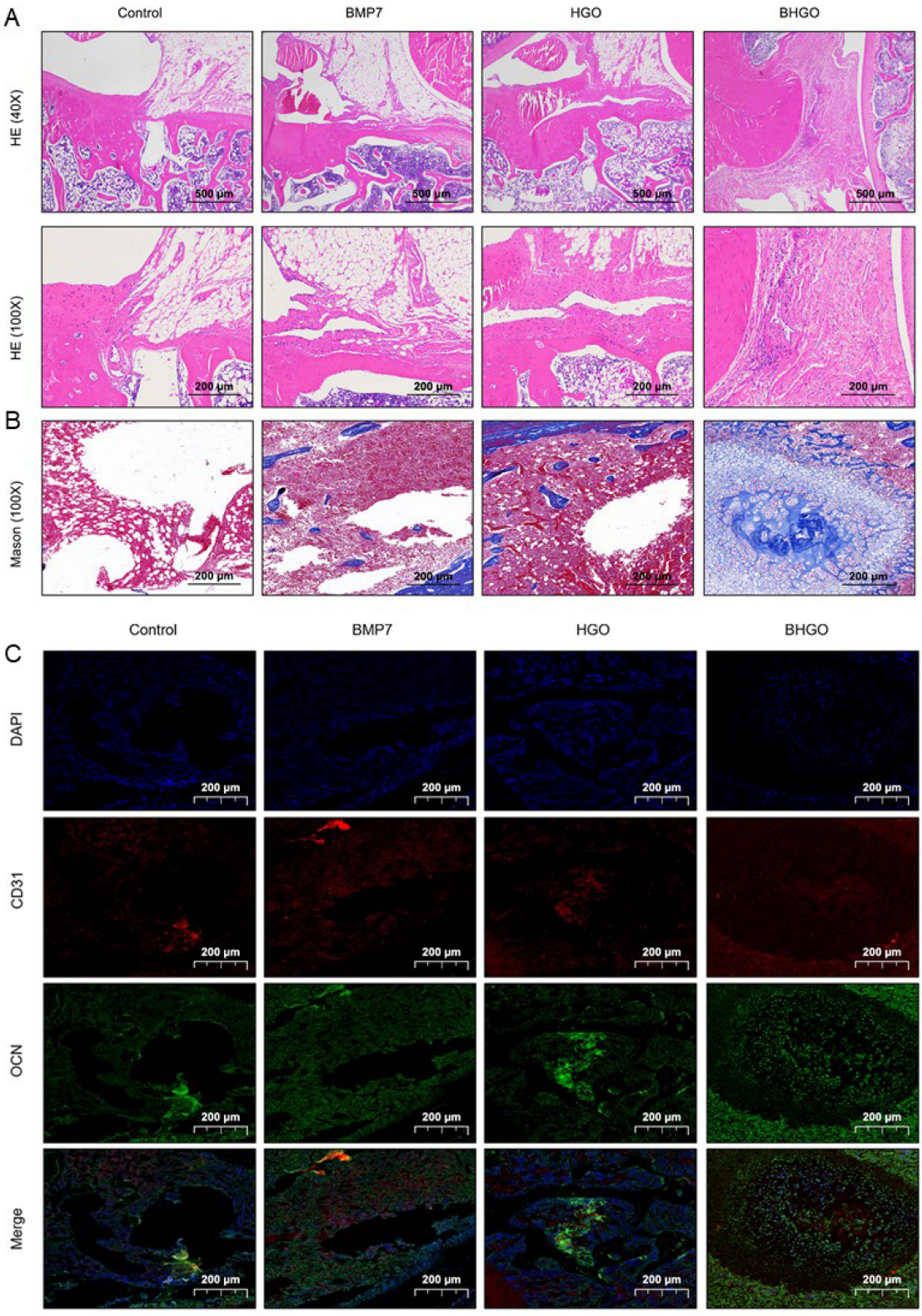

Figure 6 Histological examination of rat femurs after 4 weeks postoperation.(**A**) H&E staining results, showing increased connective and newly formed bone tissues in BMP7, HGO, and BHGO groups compared with the control group, with substantial neoplastic bone formation in the BHGO group. (**B**) Masson's trichrome staining, displaying larger neoplastic bone tissue areas in BMP7, HGO, and BHGO groups, with the BHGO group showing the largest area. (**C**) Immunofluorescence staining for osteocalcin (OCN) and CD31, indicating enhanced osteogenesis and angiogenesis in the BHGO group compared to other groups.

growth.[40] Notably, the degradation rate is inversely related to the nHAP content, as rigid nHAP Materials provide robust mechanical support to counterbalance overly rapid hydrogel degradation.[41] The biocompatibility of a stent is often the primary factor in evaluating whether a stent is capable of being utilized in the human body.[42] GelMA and OSA are commonly used scaffold materials for tissue engineering. nHAP is a major component of natural bone and can promote bone formation.[43] Cell viability and cytoskeletal studies confirmed that composite hydrogels not only provide a suitable microenvironment for BMSC survival but also facilitate their proliferation and extension. Considering the experimental findings, the HGO hydrogel with a 10% nHAP concentration was chosen as the scaffold for subsequent ex vivo osteogenesis experiments. BMP7 is an FDA-approved bone regeneration therapy with osteogenic properties.[44–46] BMP7 can promote the differentiation of BMSCs to osteoblastic stem cells and shows potent Bone generating activity in both in vitro and in vivo assays.[47,48] BMP7 were loaded into 10% HGO hydrogel scaffolds, and the ALP activity of bone marrow MSCs was elevated after 14 days which demonstrated that BHGO induces bone marrow MSCs osteogenic response. In addition, the results of alizarin red staining on day 21 showed that BMSCs produced more extracellular calcium deposits in the BHGO group compared with the blank, BMP7, and HGO groups, indicating that BHGO had a good effect on inducing osteogenic differentiation. The relative expression of bone differentiation-related proteins on day 14 was significantly higher in the BHGO group than both the BMP7 group and HGO group, further confirming that hydrogel scaffold significantly enHAPnced the osteogenic differentiation potential of BMSCs. Additionally, the animal experiment results revealed that, within the rat femoral defect model, the BHGO group exhibited the most effective bone defect repair following 8 weeks.

This study has several limitations. First, the focus was solely on the physical properties of various nHAP concentrations, neglecting the screening of GelMA and OSA ratios. Optimization of these proportions is anticipated in subsequent experiments. Second, the loading of BMP7 onto nHAP within the bioactive scaffolds was achieved through simple adsorption. Potential future studies might consider methods to fine-tune the release rate of BMP7, possibly involving proteins or particles with significant affinity for BMP7. Lastly, an increase in the number of model rats and data collection at distinct time intervals is suggested for a more comprehensive analysis.

In conclusion, composite bioactive scaffolds consisting of GelMA, OSA, nHAP, and BMP7 were successfully prepared through dual cross-linking. These scaffolds serve as effective carriers for BMSC recruitment, proliferation, and osteogenic differentiation. The results highlighted the favorable physical properties, biocompatibility, and remarkable potential of the composite scaffolds to promote BMSC osteogenic differentiation in vitro. In the rat femoral bone defect model, the BHGO scaffold exhibited superior osteogenic healing compared to the blank group, direct BMP7 injection, and HGO scaffold. Thus, the BHGO scaffold holds promise as a novel graft option for the clinical treatment of bone defects.

Conclusion

In this experimental study, we aimed to construct a safe, non-toxic, superior multi-crosslinked network and loaded osteogenic factor BMP7 for bone tissue engineering.

The introduction of nHAP optimized the performance of GelMA/OSA hydrogel. After comprehensively weighing the microstructure, mechanical properties, water absorption and swelling equilibrium, degradation rate, and cytocompatibility of different groups of hydrogels, we chose the 10% nHAP/GelMA/OSA hydrogel group as a carrier for BMP7. In cell and animal experiments, we verified that the composite hydrogel group had better ability to contribute to osteogenic differentiation and bone formation compared with the addition of simple BMP7 group and simple hydrogel scaffold group.

Therefore, this experiment is hoped to provide some help for the subsequent research on bone tissue engineering and provide a new choice for clinical bone graft substitution materials.

Abbreviations

BTE, Bone tissue engineering; ECM, Extracellular matrix; GelMA, Gelatin methacryloyl; SA, Serum alginate; OSA, Oxidized sodium alginate; Hap, Hydroxyapatite; nHAP, Nanohydroxyapatite; BMP7, Bone morphogenetic protein 7, BMSCs, Bone marrow-derived mesenchymal stem cells; OP-1, Osteogenic protein-1; OB, Osteoblast; FBS, Fetal bovine serum; EDTA, Ethylenediaminetetraacetic acid; ALP, Alkaline phosphatase.

Data Sharing Statement

The data that support the findings of this study are available from the corresponding author upon reasonable request.

Ethics Approval

The experimental procedure followed the United States National Institutes of Health Guide for the Care and Use of Laboratory Animals (NIH Publication No. 85–23, revised 1985). The study protocol was approved by the Animal Ethics Committee of Bengbu Medical College (approval number: 2022[388]).

Acknowledgments

This study was supported by the National Natural Science Foundation of China (Grant No. 81560216), the Scientific Research Program of Higher Educational Institutions in Anhui Province (Grant No. 2022AH040219), the Open Project of Key Laboratory of Bengbu Medical College (Grant No. AHTT2022A002), the Doctoral Scientific Research Initiation Fund (Grant No. KYLX100670), and the Graduate Student Research Innovation Program of Bengbu Medical College (Grant No. Bycx22095). Graduate Student Research Innovation Program (Grant No. Bycx22095).

Author Contributions

All authors made a significant contribution to the work reported, whether that is in the conception, study design, execution, acquisition of data, analysis and interpretation, or in all these areas; took part in drafting, revising or critically reviewing the article; gave final approval of the version to be published; have agreed on the journal to which the article has been submitted; and agree to be accountable for all aspects of the work.

Disclosure

The authors declare no competing interests in this work.

References

1. Wang J, Wang X, Liang Z, et al. Injectable antibacterial Ag-HA/ GelMA hydrogel for bone tissue engineering. *Front Bioeng Biotechnol*. 2023;11:1219460. doi:10.3389/fbioe.2023.1219460
2. Qi J, Yu T, Hu B, Wu H, Ouyang H. Current Biomaterial-Based Bone Tissue Engineering and Translational Medicine. *Int J Mol Sci*. 2021;22 (19):10233. doi:10.3390/ijms221910233
3. Agarwal R, García AJ. Biomaterial strategies for engineering implants for enhanced osseointegration and bone repair. *Adv drug delivery rev*. 2015;94:53–62. doi:10.1016/j.addr.2015.03.013
4. Zhang Y, Yu T, Peng L, Sun Q, Wei Y, Han B. Advancements in Hydrogel-Based Drug Sustained Release Systems for Bone Tissue Engineering. *Front Pharmacol*. 2020;11:622. doi:10.3389/fphar.2020.00622
5. Sreekumaran S, Radhakrishnan A, Rauf AA, Kurup GM. Nanohydroxyapatite incorporated photocrosslinked gelatin methacryloyl/poly(ethylene glycol)diacrylate hydrogel for bone tissue engineering. *Progress in biomaterials*. *Mar*. 2021;10(1):43–51. doi:10.1007/s40204-021-00150-x
6. Hassani A, Ç B A, Kerdar SN, et al. Interaction of alginate with nano-hydroxyapatite-collagen using strontium provides suitable osteogenic platform. *J Nanobiotechnol*. 2022;20(1):310. doi:10.1186/s12951-022-01511-9
7. Yue S, He H, Li B, Hou T. Hydrogel as a biomaterial for bone tissue engineering: A review. *Nanomaterials*. 2020;10(8):1511. doi:10.3390/ nano10081511
8. Zhao H, Zhang X, Zhou D, et al. Collagen, polycaprolactone and attapulgite composite scaffolds for in vivo bone repair in rabbit models. *Biomed Mat*. 2020;15(4):045022. doi:10.1088/1748-605X/ab843f
9. Chai S, Huang J, Mahmut A, et al. Injectable Photo-Crosslinked Bioactive BMSCs-BMP2-GelMA Scaffolds for Bone Defect Repair. *Front Bioeng Biotechnol*. 2022;10:875363. doi:10.3389/fbioe.2022.875363
10. Shi Z, Xu Y, Mulatibieke R, et al. Nano-Silicate-Reinforced and SDF-1α-Loaded Gelatin-Methacryloyl Hydrogel for Bone Tissue Engineering. *Int j Nanomed*. 2020;15:9337–9353. doi:10.2147/ijn.S270681
11. Xie Y, Gao P, He F, Zhang C. Application of alginate-based hydrogels in hemostasis. *Gels*. 2022;8(2).
12. Xing Y, Qing X, Xia H, et al. Injectable hydrogel based on modified gelatin and sodium alginate for soft-tissue adhesive. *Front Chem*. 2021;9:744099. doi:10.3389/fchem.2021.744099
13. Jiang Y, Guo S, Jiao J, Li L. A biphasic hydrogel with self-healing properties and a continuous layer structure for potential application in osteochondral defect repair. *Polymers*. 2023;15(12):2744. doi:10.3390/polym15122744
14. Li F, Li J, Song X, et al. Alginate/Gelatin Hydrogel Scaffold Containing nCeO(2) as a Potential Osteogenic Nanomaterial for Bone Tissue Engineering. *Int j Nanomed*. 2022;17:6561–6578. doi:10.2147/ijn.S388942
15. Raina DB, Liu Y, Isaksson H, Tägil M, Lidgren L. Synthetic hydroxyapatite: a recruiting platform for biologically active molecules. *Acta orthopaedica*. 2020;91(2):126–132. doi:10.1080/17453674.2019.1686865

16. Zhou Y, Liu X, She H, Wang R, Bai F, Xiang B. A silk fibroin/chitosan/nanohydroxyapatite biomimetic bone scaffold combined with autologous concentrated growth factor promotes the proliferation and osteogenic differentiation of BMSCs and repair of critical bone defects. *Regener Ther*. 2022;21:307–321. doi:10.1016/j.reth.2022.08.006
17. Qian C, Liu Y, Chen S, et al. Electrospun core-sheath PCL nanofibers loaded with nHA and simvastatin and their potential bone regeneration applications. *Front Bioeng Biotecl*. 2023;11:1205252. doi:10.3389/fbioe.2023.1205252
18. Zhang Y, Sun T, Jiang C. Biomacromolecules as carriers in drug delivery and tissue engineering. *Acta Pharma Sinica B*. 2018;8(1):34–50. doi:10.1016/j.apsb.2017.11.005
19. Mantripragada VP, Jayasuriya AC. Bone regeneration using injectable BMP-7 loaded chitosan microparticles in rat femoral defect. *Mater Sci Eng C Mater Biol Appl*. 2016;63:596–608. doi:10.1016/j.msec.2016.02.080
20. Li S, Xiaowen Y, Yang Y, et al. Osteogenic and anti-inflammatory effect of the multifunctional bionic hydrogel scaffold loaded with aspirin and nano-hydroxyapatite. *Front Bioeng Biotechnol*. 2023;11:1105248. doi:10.3389/fbioe.2023.1105248
21. Chen Y, Ma B, Wang X, et al. Potential functions of the bmp family in bone, obesity, and glucose metabolism. *J Diab Res*. 2021;2021:6707464. doi:10.1155/2021/6707464
22. Karimi Ghahfarrokhi E, Meimandi-Parizi A, Oryan A, Ahmadi N. Effects of Combination of bmp7, pfg, and autograft on healing of the experimental critical radial bone defect by induced membrane (masquelet) technique in rabbit. *Arch Bone Joint Surg*. 2021;9(5):585–597. doi:10.22038/abjs.2020.50852.2532
23. Cecchi S, Bennet SJ, Arora M. Bone morphogenetic protein-7: review of signalling and efficacy in fracture healing. *J Orthopaedic Transl*. 2016;4:28–34. doi:10.1016/j.jot.2015.08.001
24. Liu L, Li X, Shi X, Wang Y. Injectable alendronate-functionalized GelMA hydrogels for mineralization and osteogenesis. *RSC Adv*. 2018;8 (40):22764–22776. doi:10.1039/c8ra03550d
25. Wang H, Chen X, Wen Y, et al. A study on the correlation between the oxidation degree of oxidized sodium alginate on its degradability and Gelation. *Polymers*. 2022;14(9). doi:10.3390/polym14091679
26. Zhou P, Wu J, Xia Y, et al. Loading BMP-2 on nanostructured hydroxyapatite microspheres for rapid bone regeneration. *Int j Nanomed*. 2018;13:4083–4092. doi:10.2147/ijn.S158280
27. Tang S, Shen Y, Jiang L, Zhang Y. Surface Modification of Nano-Hydroxyapatite/Polymer Composite for Bone Tissue Repair Applications: a Review. *Polymers*. 2024;16(9):1263. doi:10.3390/polym16091263
28. Liu Z, Yamada S, Otsuka Y, Peñaflor Galindo TG, Tagaya M. Surface modification of hydroxyapatite nanoparticles for bone regeneration by controlling their surface hydration and protein adsorption states. *Dalton Trans*. 2022;51(25):9572–9583. doi:10.1039/d2dt00969b
29. Müller KH, Motskin M, Philpott AJ, et al. The effect of particle agglomeration on the formation of a surface-connected compartment induced by hydroxyapatite nanoparticles in human monocyte-derived macrophages. *Biomaterials*. 2014;35(3):1074–1088. doi:10.1016/j.biomaterials.2013.10.041
30. Benedini L, Laiuppa J, Santillán G, Baldini M, Messina P. Antibacterial alginate/nano-hydroxyapatite composites for bone tissue engineering: assessment of their bioactivity, biocompatibility, and antibacterial activity. *Mater Sci Eng C Mater Biol Appl*. 2020;115:111101. doi:10.1016/j.msec.2020.111101
31. Bose S, Roy M, Bandyopadhyay A. Recent advances in bone tissue engineering scaffolds. *Trends Biotech*. 2012;30(10):546–554. doi:10.1016/j.tibtech.2012.07.005
32. Ju Y, Hu Y, Yang P, Xie X, Fang B. Extracellular vesicle-loaded hydrogels for tissue repair and regeneration. *Mater Today Bio*. 2023;18:100522. doi:10.1016/j.mtbio.2022.100522
33. Tang G, Zhu L, Wang W, et al. Alendronate-functionalized double network hydrogel scaffolds for effective osteogenesis. *Front Chem*. 2022;10:977419. doi:10.3389/fchem.2022.977419
34. Alipour M, Firouzi N, Aghazadeh Z, et al. The osteogenic differentiation of human dental pulp stem cells in alginate-gelatin/Nano-hydroxyapatite microcapsules. *BMC Biotech*. 2021;21(1):6. doi:10.1186/s12896-020-00666-3
35. Makar LE, Nady N, Abd El-Fattah A, Shawky N, Kandil SH. Unmodified Gum Arabic/Chitosan/Nanohydroxyapatite Nanocomposite Hydrogels as Potential Scaffolds for Bone Regeneration. *Polymers*. 2022;14(15).
36. Ji X, Yuan X, Ma L, et al. Mesenchymal stem cell-loaded thermosensitive hydroxypropyl chitin hydrogel combined with a three-dimensional-printed poly(ε-caprolactone) /nano-hydroxyapatite scaffold to repair bone defects via osteogenesis, angiogenesis and immunomodulation. *Theranostics*. 2020;10(2):725–740. doi:10.7150/thno.39167
37. Engler AJ, Sen S, Sweeney HL, Discher DE. Matrix elasticity directs stem cell lineage specification. *Cell*. 2006;126(4):677–689. doi:10.1016/j.cell.2006.06.044
38. Yin J, Yan M, Wang Y, Fu J, Suo H. 3D Bioprinting of Low-Concentration Cell-Laden Gelatin Methacrylate (GelMA) Bioinks with a Two-Step Cross-linking Strategy. *ACS Appl Mater Interface*. 2018;10(8):6849–6857. doi:10.1021/acsami.7b16059
39. Wang Y, Cao X, Ma M, Lu W, Zhang B, Guo Y. A GelMA-PEGDA-nHA Composite Hydrogel for Bone Tissue Engineering. *Materials*. 2020;13 (17). Basel, Switzerland.
40. Zheng S, Zhong H, Cheng H, et al. Engineering multifunctional hydrogel with osteogenic capacity for critical-size segmental bone defect repair. *Front Bioeng Biotechnol*. 2022;10:899457. doi:10.3389/fbioe.2022.899457
41. Boller LA, Shiels SM, Florian DC, et al. Effects of nanocrystalline hydroxyapatite concentration and skeletal site on bone and cartilage formation in rats. *Acta Biomater*. 2021;130:485–496. doi:10.1016/j.actbio.2021.05.056
42. Gao X, Xu Z, Li S, et al. Chitosan-vancomycin hydrogel incorporated bone repair scaffold based on staggered orthogonal structure: a viable dually controlled drug delivery system. *RSC Adv*. 2023;13(6):3759–3765. doi:10.1039/d2ra07828g
43. Shi Z, Yang F, Pang Q, et al. The osteogenesis and the biologic mechanism of thermo-responsive injectable hydrogel containing carboxymethyl chitosan/sodium alginate nanoparticles towards promoting osteal wound healing. *Int J Biol Macromol*. 2023;224:533–543. doi:10.1016/j.ijbiomac.2022.10.142
44. Gillman CE, Jayasuriya AC. FDA-approved bone grafts and bone graft substitute devices in bone regeneration. *Mater Sci Eng C Mater Biol Appl*. 2021;130:112466. doi:10.1016/j.msec.2021.112466
45. Xu Q, Li Y, Zhu Y, Zhao K, Gu R, Zhu Q. Recombinant human BMP-7 grafted poly(lactide-co-glycolide)/hydroxyapatite scaffolds via polydopamine for enhanced calvarial repair. *RSC Adv*. 2018;8(48):27191–27200. doi:10.1039/c8ra05606d

46. Hayashi T, Asakura M, Kawase M, et al. Bone tissue engineering in rat calvarial defects using induced bone-like Tissue by rhBMPs from immature muscular tissues in vitro. *Int J Mol Sci*. 2022;23(13):6927. doi:10.3390/ijms23136927
47. Badr AM, Shalaby HK, Awad MA, Hashem MA. Assessment of bone morphogenetic protein-7 loaded chitosan/β-Glycerophosphate hydrogel on periodontium tissues regeneration of class III furcation defects. *Saudi Dental j*. 2023;35(6):760–767. doi:10.2147/IJN.S388942
48. Tenkumo T, Kruse B, Kostka K, et al. Development of triple-functionalized calcium phosphate nanoparticles as an advanced drug delivery system for bone tissue repair. *Rege Ther Mar*. 2024;25:49–60. doi:10.1016/j.reth.2023.11.010